



**Elucidating the mechanism of interaction between peptides
and inorganic surfaces**

Journal:	<i>Physical Chemistry Chemical Physics</i>
Manuscript ID:	CP-ART-01-2015-000088.R1
Article Type:	Paper
Date Submitted by the Author:	04-May-2015
Complete List of Authors:	Maity, Sibaprasad; Indian Institute of Science Education and Research Kolkata,, Department of Chemical Sciences Zanuy, David; UPC, Chemical Engineering Razvag, Yair; The Hebrew University of Jerusalem, Institute of Chemistry Das, Priyadip; The Hebrew University of Jerusalem, Chemistry Aleman, Carlos; Universitat Politècnica de Catalunya, Reches, Meital; The Hebrew University of Jerusalem, chemistry

ARTICLE

Elucidating the mechanism of interaction between peptides and inorganic surfaces†

Cite this: DOI: 10.1039/x0xx00000x

Sibaprasad Maity¹, David Zanuy³, Yair Razvag¹, Priyadip Das¹, Carlos Alemán^{3,4*} and Meital Reches^{1,2*}Received 00th Month Year,
Accepted 00th Month Year

DOI: 10.1039/x0xx00000x

www.rsc.org/

Understanding the mechanism of interaction between peptides and inorganic materials is of high importance for the development of new composite materials. Here, we combined an experimental approach along with molecular simulations in order to gain insights into this binding process. Using single molecule force spectroscopy by atomic force microscopy and molecular simulations we studied the binding of a peptide towards an inorganic substrate. By performing alanine scan we examined the propensity of each amino acid in the peptide sequence to bind the substrate (mica). Our results indicate that this binding is not controlled by the specific sequence of the peptide, but rather by its conformational freedom in solution versus its freedom when it is in proximity to the substrate. When the conformational freedom of the peptide is identical in both environments, the peptide will not adhere to the substrate. However, when the conformational freedom is reduced, when the peptide is in close proximity to the substrate, binding will occur. These results shed light on the interaction between peptides and inorganic materials.

Introduction

In nature, composite materials with unique properties such as high mechanical strength, optical functionality or electronic structure are formed through the specific interactions between organic (usually proteins) and inorganic materials.^{1–5} For example, the combination of the protein collagen and the inorganic mineral hydroxyapatite leads to the formation of bones which serve as a mechanical and supportive tissue.⁶ Like proteins, short peptides also exhibit specific binding affinity towards inorganic surfaces.^{7–11} The specificity of these binders (mainly peptides) is used in various applications, particularly in the design of new biomimetic hybrid materials.^{12–15} Moreover, the specific binding affinity of peptides towards inorganic substrates has been utilized to prepare nanostructured materials with novel properties and functions, such surface biocompatibility,¹⁶ drug delivery,¹⁷ crystal growth regulation,¹⁸ and nanoparticle synthesis.¹⁹

Understanding this binding mechanism will allow us to design effective biomedical materials having applications in bone-based research including bone and dentin tissue engineering, tendon and

ligament repair, and enamel formation.²⁰ Many approaches including phage display,^{21,22} quartz crystal microbalance (QCM) measurement,²³ ellipsometry²⁴ surface plasmon resonance (SPR)^{23,25} and other methods^{26–28} have been employed to assess the affinity of peptides towards targeted inorganic surfaces.

Although, these methods indeed identify many peptide sequences that bind to certain surfaces, the reason for the propensity of a certain sequence to a certain substrate is still not clear. This is because completely different sequences can bind a specific substrate. Single molecule force spectroscopy using atomic force microscopy (AFM) may provide information about peptide–inorganic surface interaction at single molecular level. Force spectroscopy allows the detailed study of molecular interactions that are not available with other techniques.^{29,30} This technique has been extensively used to investigate the interaction between biotin and–avidin,^{31,32} DNA strands,³³ antigen–antibody,³⁴ lectin–carbohydrate,³⁵ bacterial adhesion,³⁶ peptide–cell interaction³⁷ etc. Using this technique Dupres *et al.* have demonstrated the interaction of the peptide D-Ala-D-Ala with stainless steel.³⁸ Utilizing single molecule force spectroscopy and theoretical approaches Krysiak *et al.* determined the monomeric desorption rate of homopolypeptide from flat surfaces.³⁹ Recently, we have measured single molecular interaction between individual amino acids residues and inorganic surfaces.⁴⁰ This manuscript describes the utilization of single molecule force spectroscopy measurements for elucidating the mechanism of peptide binding to inorganic surfaces. Specifically, we studied the role of each amino acid in a peptide sequence which binds mica. Furthermore, theoretical description of selected peptides among those studied experimentally, has been used to rationalize the

1. Institute of Chemistry, The Hebrew University of Jerusalem, 91904, Jerusalem, Israel.

2. The Center for Nanoscience and Nanotechnology, The Hebrew University of Jerusalem, 91904, Jerusalem, Israel.

3. Department of Chemical Engineering, Universitat Politècnica de Catalunya, ETSEIB, 08028, Barcelona, Spain.

4. Center for Research in Nano-Engineering, Universitat Politècnica de Catalunya, Campus Sud, Edifici C', C/Pasqual i Vila s/n, Barcelona E-08028, Spain

† Electronic supplementary information (ESI) available: Experimental procedures, Additional histograms, and molecular simulation. See DOI: 10.1039/x0xx00000x

binding affinity of the different peptides. We demonstrate that an approach based on the combination of results derived from single molecule force spectroscopy and atomistic computer simulations can be used to rationally design more efficiently hybrid organic-inorganic materials.

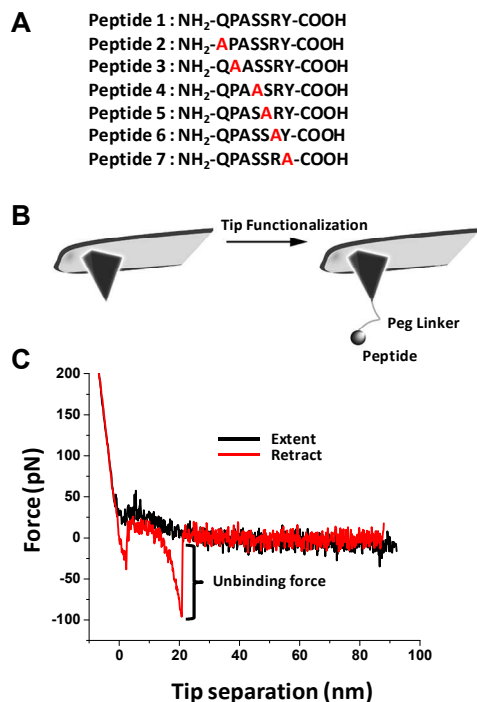


Fig. 1 (A) The sequences of the studied peptides, (B) Schematic representation of the peptide-functionalized AFM tip, (C) A representative F-D curve for the interaction of peptide 1 with mica.

The interactions between a peptide and a certain surface can be affected by several parameters. These parameters are related both to the properties of the peptide (sequence and structure) and to the properties of the surface (surface topography, roughness and chemistry). To simplify this problem we chose to study a system in which the peptide sequence is as short as possible (seven amino acids) and the substrate is mica which is atomically flat. A short peptide, NH₂-Gln-Pro-Ala-Ser-Ser-Arg-Tyr-COOH, which binds strongly to mica was previously identified by phage display.⁴¹ To elucidate the role of each amino acid in the binding propensity of this specific peptide towards mica we performed alanine scan and studied the adhesion of each peptide by single molecule force spectroscopy (Fig. 1A). Each peptide chemically modified Si₃N₄ cantilevers with silicon tips as described in the experimental section (Fig. 1B).⁴⁰ Polyethylene glycol (5000 Da) linked between the tip and the peptide since it (i) allows the peptide to orient freely on the tip, (ii) overcomes the danger of the peptide being compressed between the tip and the substrate during contact, and most significantly (iii) is a soft molecule with nonlinear elasticity and therefore allows us to distinguish between the nonspecific interactions of the tip with the substrate and the binding of the peptide to the substrate.⁴²⁻⁴³

EXPERIMENTAL SECTION

Materials and Methods

Silicon nitride (Si₃N₄) AFM cantilevers with silicon tips (MSNL10, nominal cantilevers radius ~ 2 nm) were purchased from Bruker (Camarillo, CA). Methyltriethoxysilane (MTES) was purchased from Acros Organics (New Jersey, USA). 3-(Aminopropyl) triethoxysilane and Triisopropylsilane were purchased from Sigma-Aldrich (Jerusalem, Israel). N-ethyl-diisopropylamine, triethylamine and piperidine were obtained from Alfa-Aesar (Lancashire, UK). Fluorenylmethyloxycarbonyl-PEG-N-hydroxysuccinimide (Fmoc-PEG-NHS), 5000 Da was purchased from Iris Biotech GmbH (Deutschland, Germany), Trifluoro acetic acid (TFA) and acetic anhydride from Merck (Darmstadt, Germany). The peptides were purchased from GL Biochem (Shanghai, China). All peptides had an Fmoc protecting group at the N terminus and protecting groups on the side chains (where required). Trityl (Trt) protected the side chain of glutamine, pentamethyl-2,3-dihydrobenzofuran-5-sulfonyl (Pbf) protected the side chain of arginine and tertiary butyl (tBu) protected the side chain of serine and tyrosine (see supporting information). The Mica substrates (9.9 mm diameter) were purchased from TED PELLA, INC. (Redding, California, USA).

Tip Functionalization

The chemical modification of the AFM tip was based on our previous report.⁴⁰ The AFM cantilevers were cleaned by dipping in ethanol for 20 minutes. After drying at room temperature, they were treated by O₂ Plasma (Atto, Diener Electronic, Ebhausen, Germany) for 5 minutes. The tips were then suspended above (3 cm) a solution containing methyltriethoxysilane and 3-(aminopropyl) triethoxysilane in a ratio of 15:1 (v/v) in a desiccator which was connected to vacuum pump. The desiccator was vacuumed for 2 hours to form a monolayer of these two types of mixed silane compounds. The tips were then dried on a hot plate for 10 minutes at 70°C under atmospheric conditions. After cooling at room temperature, the tips were immersed in a solution of Fmoc-PEG-NHS (MW 5000) at a concentration of 5 mM in chloroform containing 0.5% (v/v) triethylamine for 1 hour at room temperature. The tips were then extensively washed with chloroform and dimethylformamide (DMF). Deprotection of the Fmoc group of the attached PEG molecules was performed by dipping the tips in 20% piperidine(v/v) in DMF for 30 minutes. This was followed by washing with DMF and N-methyl-2-pyrrolidone (NMP). The amine groups of the attached PEG molecule were then coupled with the carboxyl group of the desired peptide by dipping the tips into 2 mL solution containing 40 mg of the protected peptides (N terminal and side chains), 15 mg 2-(1H-benzotriazol-1-yl)-1,1,3,3,-tetramethyluronium hexafluorophosphate (HBTU) and 5 µL of N-Ethyl-diisopropylamine (DIPEA) in N-Methyl-2-pyrrolidone (NMP) for 2 hours. After that the tips were extensively washed with NMP. The NH₂ groups, which did not react, were protected by acetyl group by dipping the tips in a solution containing 45 µL N-Ethyl-diisopropylamine and 98 µL of acetic anhydride in 1 mL NMP. The side chains of peptide were deprotected by treating the tips with a solution containing 95%

TFA, 2.5% triisopropylsilane and 2.5% water for 1 hour, followed by washing with chloroform and DMF. The Fmoc group of the peptide was deprotected by dipping the tips in 20% Piperidine(v/v) in DMF for 30 minutes. Finally the peptide functionalized tips were repeatedly washed with DMF, chloroform, 50% ethanol, water and then dried in air.

Surface Preparation

Mica substrates (9.9 mm diameter) were cleaved before each use using scotch tape. Then the surfaces were washed with triple distilled water (TDW).

Single Molecule Force Spectroscopy Measurements

Force spectroscopy measurements were carried out in TDW at 298K, using a commercial AFM, a NanoWizard® 3 (JPK Instruments, Berlin, Germany). The AFM cantilevers with spring constants ranging from 10 to 30 pN nm⁻¹ were calibrated by the thermal fluctuation method (included in the AFM software) with an absolute uncertainty of approximately 10%.⁴⁴ Measurements were obtained by approaching the peptide functionalized tip to the substrate until it was in contact with the substrate with a compression force of ~200 pN and then immediately retracting the tip at various speeds, from 0.2 to 0.6 μm/sec, for a distance of ~200 nm.

Data Analysis

Prior to analysis, the deflection values (V) were converted to force by multiplying the photodiode sensitivity (V/m) and by the experimentally determined spring constant.⁴⁵ Only single adhesion events were taken into account (between 10%-30 % of the curves) ensuring that >95% probability that the adhesion event was mediated by a single bond.⁴⁶ To calculate the apparent loading rate, we fitted at least 50 force vs. distance curves with the worm like chain (WLC) model just prior to raptures to obtain a set of loading rates, which were then used for preparing histograms of apparent loading rates. The unbinding forces between the peptides and mica were derived from the jump in force following the separation of the cantilever from the substrate. This was done using the JPK data processing software (JPK Instruments, Berlin, Germany).

Peptide Modification

To study the adsorptive nature of these peptides to mica and to perform fourier transform infrared (FT-IR) analysis, all the protecting groups associated with the side chains and the Fmoc group at the N terminal were removed. First, the Fmoc group was removed with 20% piperidine solution in DMF, followed by lyophilization. The product was washed with hexane repeatedly (five times) to remove any by-products and dried under vacuum. To remove all other protecting groups on the side chains, the product was treated with a solution containing 95% TFA, 2.5% triisopropylsilane and 2.5% water under shaking for 3 hours. Then, the TFA and water were evaporated in vacuum overnight. The solid product we obtained was treated with cold diethyl ether followed by decantation and washing with diethyl ether. The product was precipitated out by adding cold diethyl ether in TFA. Finally, the product was centrifuged and purified by reverse phase HPLC. The

purity of the peptides were then confirmed by MALDI-TOF mass spectroscopy.

Fourier Transform Infrared (FTIR) Spectroscopy

1 mg of each purified peptide was dissolved in 1 mL of TDW. These stock solutions were then diluted to a final concentration of 0.5 mg/mL and 0.1 mg/mL. A 30 μL of each peptide solution was drop cast on a CaF₂ window and dried under vacuum. The peptide deposits were then re-suspended with D₂O and subsequently dried under vacuum. The re-suspension procedure was repeated three times to ensure maximal hydrogen-to-deuterium exchange. Data was collected using a Nicolet 6700 FT-IR spectrometer (Thermo Fisher Scientific, MA, USA). The measurements were taken using a 4 cm⁻¹ resolution and averaging 3000 scans. The deconvolution was performed using MagicPlot.

Topography Analysis

Freshly cleaved (both sides) mica was dipped for 1 hour in each peptide solution at three different concentrations. Then, the surfaces were washed with TDW, followed by sonication in TDW for 5 minutes to remove unabsorbed peptides. Surfaces were then cleaned with TDW and dried with dry nitrogen. Topographical analysis of the surfaces were performed by AFM using AC mode. Si₃N₄ cantilever probes (Bruker, Camarillo, CA) with a spring constant of 3 N/m and a resonance frequency of 75 kHz were used for imaging.

Molecular Simulations

Molecular dynamics (MD) simulations were carried out to obtain microscopic information about the interactions involved in the binding of the selected peptides to mica. Peptides were built and represented using the standard parameters of the latest version of AMBER force field.⁴⁷ Peptides were capped at the N-terminal site with an inactive acetyl group, mimicking the coupling to the polymeric coating of the AFM tip in the experiments. The remaining titratable groups were set to their ionized forms at pH=7.0.

The mica K₁[Si₃Al₁O₈][Al₂O₂(OH)₂] surface was represented using the force-field parameters reported by Heinz and co-workers, which successfully describes the unit cell properties of this inorganic material.⁴⁸⁻⁴⁹ The mica super cell model, kindly supplied by Dr Heinz, was adapted to the dimensions of the simulation box: *a*=76.793 Å and *b*=80.009Å. The thickness (*i.e.* extension in the *c*-direction) of this sheet model was 6.7 Å. In order to avoid the bending of the mica sheet during the MD simulations, the position of the ions at the surface was kept fixed during the simulations. Water molecules, which were represented using the TIP3P model,⁵⁰ were added to the simulation box to fill up the space not occupied by the surface and the peptide. The amount of water molecules, which was equalized for all studied systems, was 15,608. All simulations were performed using the NAMD 2.9 program.⁵¹ Atom pair cut-off distance was set at 14.0 Å to compute the van der Waals interactions. In order to avoid discontinuities in the potential energy function, non-bonding energy terms were forced to slowly converge to zero, by applying a smoothing factor from a distance of 12.0 Å. Beyond cut off distance, electrostatic interactions were calculated by using Particle Mesh of Ewald (PME), with a points grid density of the reciprocal space of 1 Å⁻³.⁵² The numerical integration step was set at 2

fs. Bond lengths involving hydrogen atoms were constrained using the rattle algorithm.⁵³ Periodic boundary conditions using the nearest image convention were applied in all directions for the assemblies in solution. The non-bonded pair list was updated every five steps. Before equilibration cycles, each system was submitted to 5000 steps of energy minimization (Newton Raphson method). After this, the water phase was equilibrated by applying 10^5 steps of heating and subsequent stabilization at 298 K using NVT conditions. The Berendsen thermostat with a relaxation time of 1 ps was used.⁵⁴ Then, the solvent density was equalized to its optimum value using 250000 steps of anisotropic NP_zT simulation at 298 K. This strategy kept the area of the studied surface constant while the solvent box was allowed respond to the pressure fluctuation on the z-axis. These conditions were achieved by combining the Nose–Hoover⁵⁵ piston combined with the piston fluctuation control of temperature implemented for Langevin Dynamics.⁵⁶ The pressure was kept at 1.01325 bars while the oscillation period and the piston decay time were set at 1 and 0.001 ps, respectively. The piston temperature and the damping coefficient were set at 298K and 2 ps, respectively. During these equilibration cycles, both the solid phase particles and the peptide were kept frozen. Once the simulation box dimensions were stabilized, the final equilibration cycles started. After unfreezing the peptide, 150000 steps of anisotropic NP_zT simulation were run to finally tune each model system to the simulation conditions. The last snapshot of this latter run was the starting point of 10 ns of production time. Production runs were performed under the same conditions previously mentioned for the NP_zT equilibration. In order to ensure the reproducibility of the results, simulations were performed in triplicate for each system.

Results and Discussions

Single molecule force spectroscopy

Single molecule force spectroscopy experiments were performed by recording the force vs. separation distance curves between a peptide functionalized AFM tip and a flat surface (mica). These curves were recorded at 298K in TDW, pH 7.1. Fig. 1C shows a typical Force-Distance (F-D) curve for the interaction between peptide **1** and mica. The first peak in the retract curve indicates nonspecific interactions between the tip and mica. The second peak corresponds to the specific interaction of peptide **1** with mica. Several hundred (800–1500) of such F–D curves were recorded from at least two modified AFM cantilevers, functionalized with each of the peptides, and accounted for 10–30% of the specific binding events. This low probability of events provides evidence that the measurements are indeed based on single-molecule interactions with the substrate.⁵⁷ The curves that presented successful specific binding events were then fitted to the WLC model and the retracting forces were utilized to set up a histogram of the unbinding forces. A Gaussian fit applied to these histograms indicated the average unbinding force, which is known as the most probable force (MPF). In addition, the F-D data was collected at different loading rates for each cantilever and the MPF was calculated for each batch (Fig. 2). Our results revealed that all peptides, except peptide **3**, interacted significantly with mica. Peptide **3** did not exhibit any detectable interaction with the

substrate. The limit of detection for this system is 20 pN. To ensure this insignificant interaction of peptide **3** with mica, we repeated the tip functionalization process four times and performed additional force measurement at the same conditions as for the other peptides. All our attempts supported this result. The other peptides (**1**, **2**, **4**, **5**, **6** and **7**) successfully bound to mica. To compare these six peptides, the MPF of each was calculated at approximately the same apparent loading rate. These were done by calculating the slopes of the curves just prior to unbinding events.⁵⁸

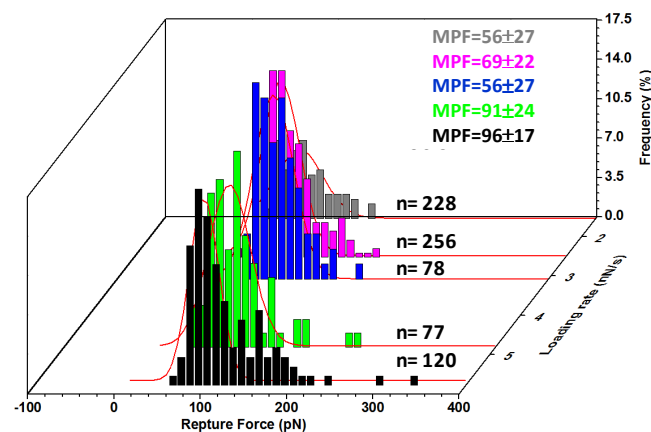


Fig. 2 Waterfall representation of a pull-off force histogram for the interaction between peptide **1** and mica at different apparent loading rates (1.54 nN, 2.52 nN, 3.08 nN, 4.82 nN and 5.80 nN) at 298K in TDW. The red lines represent the Gaussian fit for each histogram. *n* is the number of curves used for generating a histogram.

At an apparent loading rate of 3.1 ± 0.6 nN/s, peptide **1** bound to mica with a MPF value of 80 ± 23 pN, whereas peptide **2** showed a MPF of 119 ± 33 pN at apparent loading rate of 3.8 ± 0.9 nN/s (Fig. S1†). Similarly peptide **4**, **5**, **6** and **7** bound the mica substrate with a MPF of 72 ± 17 pN, 120 ± 35 pN, 92 ± 30 pN and 85 ± 35 pN at an apparent loading rate of 3.2 ± 0.7 nN/s, 3.3 ± 0.8 nN/s, 2.9 ± 0.7 nN/s and 3.5 ± 1.1 nN/s, respectively (Fig. S1†).

To gain more insights into the binding nature of these peptides we used the Bell-Evans approach.^{25,59} This procedure predicts a logarithmic dependence of the most probable force with the apparent loading rate through the following equation:

$$F = \frac{k_B T}{X_b} \ln \left(\frac{X_b r}{k_B T K_{off}} \right)$$

Where *F* is MPF, *K_B* is the Boltzmann constant, *T* is temperature in Kelvin, *X_b* is the distance of the energy barrier that needs to be overcome for unbinding along the direction of applied force, *K_{off}* is the dissociation rate at equilibrium, and *r* is the apparent loading rate. For specific peptide-substrate interactions, when the MPF from several apparent loading rates (*r*) was plotted as a function of $\ln(r)$, the equilibrium parameters *X_b* and *K_{off}* were extracted as the intercept and the slope of a linear fit, respectively (Fig. 3). Similar plots and extrapolations of kinetic parameters were performed for all the peptides as summarized in Table 1

Table 1: Kinetic parameters for the peptide-mica binding events for all the studied peptides. ND= Non detectable.

Peptide	X_b (Å)	K_{off} (s^{-1})	τ_0 (s)
1	1.34	8.02	0.124
2	2.85	0.07	14.285
3	ND	ND	ND
4	1.22	10.9	0.092
5	0.88	5.55	0.180
6	1.51	3.61	0.277
7	1.22	8.17	0.122

The distances of energy barrier X_b for the six peptides ranged from 0.88 Å to 2.85 Å (Fig. 3). The dissociation rate constants K_{off} at equilibrium were $8.02s^{-1}$, $0.07s^{-1}$, $10.90s^{-1}$, $5.55s^{-1}$, $3.61s^{-1}$ and $8.17s^{-1}$ for peptide 1, 2, 4, 5, 6 and 7, respectively (Fig. 3). The lifetimes of bond (τ) between each peptide and mica calculated accordingly as $\tau = 1/K_{off}$. The calculated bond lifetime for peptide 1, 2, 4, 5, 6 and 7 and mica were 0.124s, 14.285s, 0.092s, 0.180s, 0.277s and 0.122s, respectively.

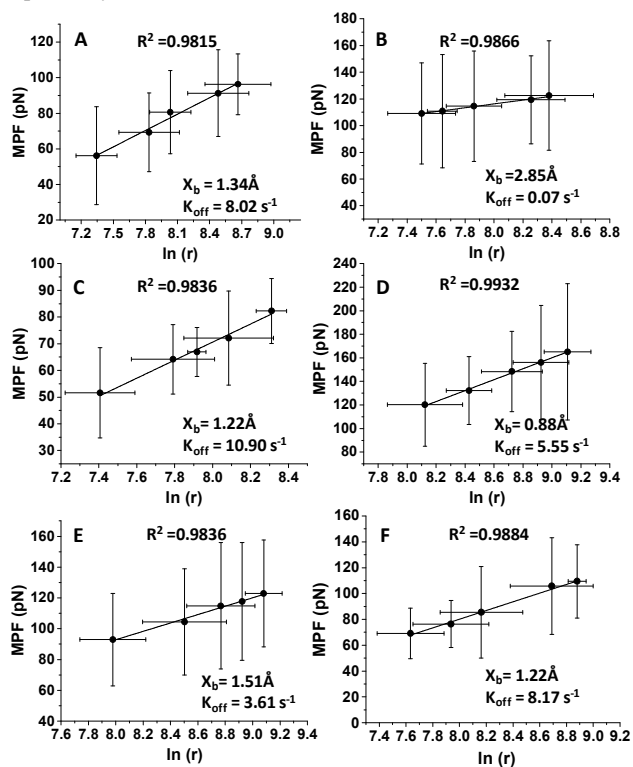


Fig. 3. The kinetic parameters were extrapolated from the linear plot of the force vs logarithm of the apparent loading rate for peptide (A) 1, (B) 2, (C) 4, (D) 5, (E) 6 and (F) 7. The y and x error bars represent the variance of the Gaussian fit and the standard deviation of the apparent loading rate (r) calculated from at least 50 different F–D curves. R^2 represents the quality of linear fitting.

Topography study

To obtain a more visualized image of the binding affinity of the peptides to the substrate in bulk, we incubated a mica substrate in a peptide solution of different concentrations (0.1, 0.5 and 1.0 mg/mL)

for one hour. We then used AFM operating in an AC imaging mode to characterize the topography of the substrates. Fig. 4 shows the adsorbed peptides (peptides 1-7) at a concentration of 0.5mg/mL. The AFM images indicated that all peptides adsorbed onto the mica. In the case of peptides 1, 2, 4 and 5 a slightly higher layer adsorbed on the mica surface when compared to peptides 3, 6 and 7. AFM topography analysis for the other peptide concentrations showed the same trend (Fig. S2[†]). These results further emphasize the major differences between the behavior of a peptide at a single molecule level and in bulk. In bulk, the peptide monomers can aggregate and form new molecular arrangements. Therefore, this comparison between bulk and single molecule is essential.

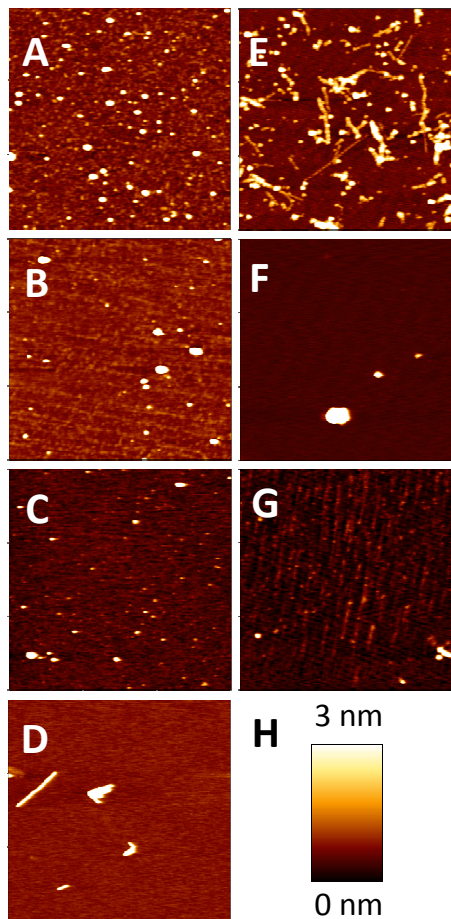


Fig. 4. AFM images of peptide 1-7 adsorbed onto mica surface at a concentration of 0.5 mg/mL after one hour of incubation. (A) peptide 1, (B) peptide 2, (C) peptide 3, (D) peptide 4, (E) peptide 5, (F) peptide 6 and (G) peptide 7. The scan size of all images was $3 \times 3 \mu\text{m}$. (H) Represents the scale of the Z axis.

Fourier Transform Infrared (FTIR) study

Peptide 3 differs from peptide 1 in its third amino acid. In peptide 3 the amino acid alanine replaced proline. The distinctive cyclic structure of proline gives an exceptional conformational rigidity compared to other natural amino acids. We, therefore, assumed that the adhesion of peptide 1 to mica is determined by the peptide conformation. To test this hypothesis we analyzed the secondary

structure of peptides 1-7 using FT-IR analysis and deconvoluted each spectrum. The spectra of all peptides had a minor peak between 1728-1734 cm^{-1} attributed to C=O stretching frequency of carboxylic group at the C termini.⁶⁰ This peak was the smallest for peptide 6 due to the high intensity of the peak in the amide I region (1657 cm^{-1}). The FT-IR spectrum of peptide 1 had a major peak at 1660 cm^{-1} . This peak is usually attributed to β -turns and therefore may imply that the peptide does not have a defined secondary structure (Fig. 5A).⁶⁰ The spectra for peptide 2, 6 and 7 had a major peak at 1657 or 1658 cm^{-1} representing a α -helix secondary structure (Fig. 5B, F and G). Notably, peptide 3 had two major peaks, one at 1658 cm^{-1} which corresponds to a α -helix secondary structure and another one at 1616 cm^{-1} which may suggest either an extended hydrated structure or β -sheet (Fig. 5C).⁶¹ This may suggest that peptide 3 has a distinct secondary structure. Peptide 4 showed two major peaks at 1657 cm^{-1} and 1685 cm^{-1} which suggest a α -helix and β -turn respectively.^{60,62} The spectrum of peptide 5 consisted of very small peaks at 1616 cm^{-1} and 1644 cm^{-1} with a major peak at 1662 cm^{-1} that corresponds to β -turn.^{60,61}

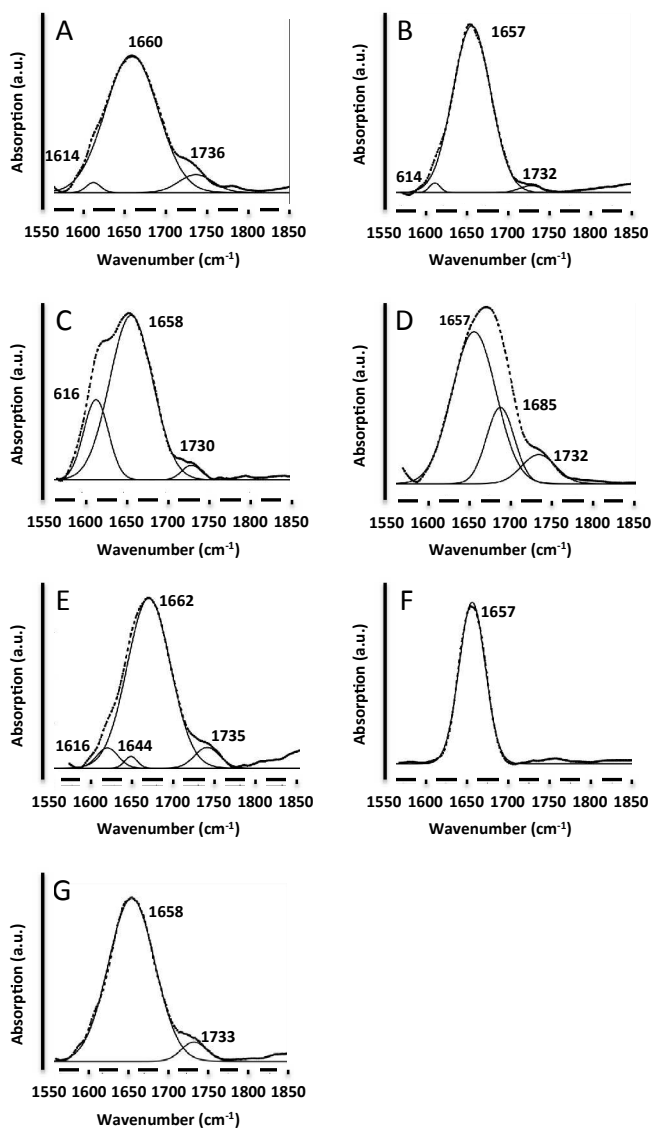


Fig. 5 Deconvoluted FT-IR spectra of peptide 1-7 (A-G). The dash line indicates the original FTIR spectra and the solid line represents the deconvoluted curves with Gaussian function.

Molecular Simulation

To gain more insights on the role of structure versus sequence in these peptide-surface interactions we performed MD simulation. To examine different aspects of the adsorption of peptides 1, 3 and 4 to mica, two independent simulations (A and B, each one by triplicates) were performed for each studied peptide. In the first simulation (denoted MD#A, where # refers to 1, 3 or 4), the peptide was set on the surface during the set up phase, whereas the initial position of the peptide was sufficiently far away from the surface (*i.e.* at least twice of the cutoff distance, $2 \times 14 \text{ \AA} = 28 \text{ \AA}$) in the second simulation (labeled as MD#B). According to this, MD#A simulations represent the peptides adsorbed onto mica while MD#B represents solvated peptides that remain at distances relatively close the surface but without adsorption. Inspection of the temporal evolution of the distances between the center of masses of each peptide residue and the mica surface, calculated using the normal vectors, indicated that these representations are maintained during MD#A and MD#B simulations in all cases (Fig. S3†). Comparison of the conformational preferences of each peptide, the energetic associated to the peptide structure and the existing peptide-surface and peptide-solvent interactions have provided accurate explanation for the experiments discussed in the previous section. The conformation of peptide 1, 3 and 4 was examined considering the different scenarios described in MD#A (peptide bound to the surface) and MD#B (peptides in solution far from the surface) simulations. The temporal evolution of the radius of gyration (R_g), which provides a direct indication of the molecular flexibility, is displayed in Fig. 6 for the three examined peptides. These results reflect that the conformational freedom of peptide 1 is very small, independently of its relative position with respect to the mica surface. Thus, the average R_g values determined from the whole MD1A and MD1B trajectories are very similar and show small standard deviations (5.57 ± 0.35 and $5.52 \pm 0.35 \text{ \AA}$, respectively). Peptide 3 exhibits a totally opposite behavior.

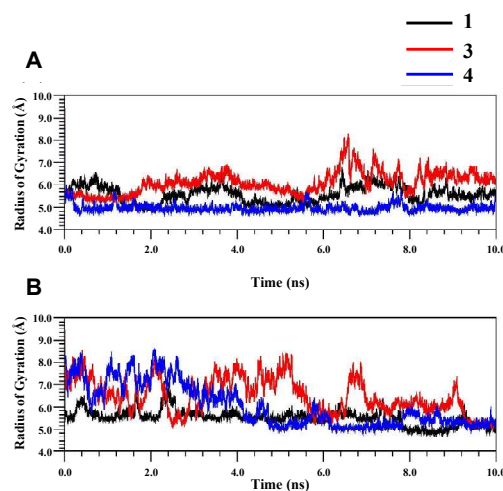


Fig. 6 Temporal evolution of the radius of gyration determined for peptides **1**, **3** and **4** using the snapshots recorded in (A) MD#A and (B) MD#B trajectories.

Thus, the intrinsic conformational flexibility of this compound, which is reflected by the large standard deviation of the average R_g derived from MD3B (6.06 ± 0.97 Å), is not mitigated upon deposition onto the mica surface (6.10 ± 0.59 Å for MD3A). The behavior of peptide **4** is intermediate between those of **1** and **3**. Thus, conformational flexibility of **4** decreases drastically upon interaction with the mica surface (4.97 ± 0.17 and 6.06 ± 0.87 Å for MD4A and MD4B, respectively), suggesting that molecular rigidity is a key factor in the binding process. These features are fully supported by the accumulated Ramachandran plots displayed in Fig. S4†. For peptide **1** the conformation of the six amino acid remains at the helical region of the Ramachandran map during the whole trajectories (Fig. S6a†), this helical arrangement favoring not only the interaction of the backbone with the mica surface but also of the side groups. In contrast, the lack of a regular conformation for peptide **3**, which is very flexible, reduces drastically the affinity towards the inorganic surface through a proper distribution of the backbone and side groups (Fig. S6b†). Finally, the conformational preferences of peptide **4** largely depends on its interaction with mica, changing from a unfolded state relatively similar to that of **3** to a regular helix (Fig. S6c†) similar to that of **1** upon deposition onto the inorganic surface. Comparison of these results with experimental observations indicates that a necessary condition for the peptide to bind mica is a limited conformational mobility. A clustering analysis was used to categorize the different conformations recorded for each peptide in a list of *unique* conformations. The list was organized according to an increasing energy order. Unique minimum energy conformations were identified using the virtual dihedral angles defined by the C atoms of the peptide, which characterize the peptide backbone conformation, and both hydrogen bond and salt bridge interactions. The latter interactions were defined on the basis of the following geometric criteria: a) for salt bridges, the distance between the centers of the interacting groups shorter than 4.5 Å; b) for hydrogen bonds, the H...X distance (with X= O or N) shorter than 2.5 Å and the $\angle Y-H \cdots X$ angle higher than 120°. Two conformations were considered different when differing in at least one of their virtual dihedral angles by more than 60° or in at least one of the above mentioned interactions. All these criteria were found to be successful for the identification of bioactive clusters in linear peptides.⁶³⁻⁶⁵ Table 3 summarizes the main results of the clustering analysis while details about the existing interactions are provided in Table S1†.

In MD#B simulation the peptides **1**, **3** and **4** explored up to 695, 1554 and 565 unique conformations, respectively. These numbers dropped by around a half in MD#A. In spite of this considerable reduction, the number of unique conformations found in MD3A is still 52% and 58% higher than those explored in MD1A and MD2A, respectively, corroborating the high conformational freedom of **3** with respect **1** and **4**. Obviously, unique conformations cover a wide range of relative energies (ΔE) and, therefore, only a very low amount (< 5%) of them is representative. Table 2 includes the

number of unique conformations with relative energy $\Delta E < 10$ kcal/mol calculated with respect to the global minimum of each set of simulations. As can be seen, the number of these conformations, here after denoted representative, is 18 and 11 for MD1A and MD4A, respectively, increasing to 25 for MD3A. This feature is in excellent agreement with the experimental observation that peptide **3** cannot bind mica.

Table 2. Clustering analyses of MD#A and MD#B simulations, where # corresponds to peptides **1**, **3** and **4**. The first column indicates the total number of unique structures identified for every simulation while the second column only includes the representative conformations (i.e. those within a relative energy gap of 10 kcal/mol with respect to the absolute minimum). The third column shows the total residence time (τ ; in ns) of all representative conformations, which has been obtained as the sum of their life-times.

Simulation	Unique	Representative	τ
MD1A	361	18	5.026
MD1B	695	12	1.392
MD3A	758	24	0.996
MD3B	1554	25	0.576
MD4A	315	11	5.060
MD4B	565	489	9.606

In addition, Table 3 shows the particular behavior of peptide **4**, which is very flexible when it is surrounded by the solvent and very restricted when it is adsorbed onto mica (*i.e.* 489 (MD4B) versus 18 (MD4A) representative conformations). The sum of the life times of all representative conformations for each simulated peptide, which has been denoted τ in Table 3, also provides relevant information about the binding. Consistently with its conformational variability, τ is very low (< 1 ns) peptide **3**. In contrast, τ is very high for peptide **4**, independently of the binding to the mica surface.

For MD4B, the very high value of τ (~9.6 ns) together with the impressive number of representative conformation (489) indicates that the substitution of serine by alanine modifies drastically the potential energy hypersurface of peptide **1**, becoming significantly flatter (*i.e.* the energy gaps between unique conformations decreases with respect to MD1B, which only shows 12 representative conformations with $\tau \approx 1.4$ ns). For peptide **4** the value of τ decreased to 5.1 ns upon binding to the inorganic surface, being practically identical to that obtained for MD1A (~0.5 ns). This feature suggests that the mica surface affects drastically on the shape of the potential energy hypersurface, favorable interactions between the peptide and the surface being possible only for some conformational patterns. This hypothesis is supported by both the drastic reduction of representative conformations associated to the binding of peptide **4** (*i.e.* from 489 in MD4B to 11 in MD4A) and the similarity between the number of representative conformations in MD1A and MD4A. Another interesting feature is that τ is very low (~1.4 ns) for MD1B, suggesting that that the short life times of these conformations does not represent an obstacle to effectively interact with the surface for subsequent binding.

In order to provide a clearer picture of the energy associated with the binding of peptides **1**, **3** and **4** to mica, the energy analyses have been carried out considering the following three contributions: (i) the intramolecular peptide non-bonding interactions (*i.e.* electrostatic and van der Waals interactions beyond three consecutively bonded atoms), $E_{p,nb}$, which takes into account the most relevant contribution to the internal energy changes associated to conformational variability; (ii) the interaction of the peptide with the mica surface, E_{p-m} ; and (iii) the interaction of the peptide with solvent molecules, E_{p-w} . Accordingly, the contribution associated with the interaction between the mica surface and the solvent molecules has been omitted from the present analyses. These interactions are expected to play a crucial role in the evaluation of the free energy profiles associated with the binding process, which is out of the scope of the present study. However, preliminary calculations with a reduced set of snapshots revealed that mica – water interactions are not necessary to explain the experimental observations described in this work, their role being negligible. In addition, the intramolecular contribution associated with the peptide bonding interactions (*i.e.* stretching, bending and torsional strain) has been found to be negligible when peptides located at the same environment are compared and, therefore, has been omitted for clarity.

The averaged energy contributions are summarized in Table 3. As it can be seen, differences between the sum of $E_{p,nb}$, E_{p-m} and E_{p-w} contributions (Σ) for MD#A and MD#B favor the adsorption of peptides in all cases, including peptide **3**. Despite the fact that the results for this peptide are apparently in disagreement with experiments observations, detailed analysis of the different contributions reveals qualitative agreement with AFM observations. The lowest $\Delta\Sigma$ corresponds to peptide **1**, -53 kcal/mol. This significant stabilization is due to the highly favorable peptide-surface interactions, which compensate the unfavorable desolvation term associated with the adsorption process ($\Delta E_{p-w} = +70$ kcal/mol) and the small conformational strain induced by the charged group of the inorganic surface. Indeed, inspection of the temporal evolution of the E_{p-m} term derived from MD1A and MD1B reveals that the ΔE_{p-w} contribution is favorable during the whole trajectory (Table 3).

Table 3. Sum of the three energy contributions ($\Sigma = E_{p,nb} + E_{p-m} + E_{p-w}$; in kcal/mol), non-bonding intramolecular energy of the peptide ($E_{p,nb}$; in kcal/mol) and interaction energy between the peptide and the mica surface (E_{p-m} ; in kcal/mol) calculated for all the studied systems. Standard deviations are displayed for all the averages. The $\Delta\Sigma$, $\Delta E_{p,nb}$ and ΔE_{p-m} values correspond to the difference between the states described in MD#A and MD#B simulations.

Peptide	MDB		
	Σ^a	$E_{p,nb}$	E_{p-m}
1	-465±24	-89±19	-1±2
3	-480±24	-99±22	-10±17
4	-458±18	-75±15	0±1
	MDA		
	Σ	$E_{p,nb}$	E_{p-m}
1	-518±19	-82±12	-129±31
3	-504±19	-88±14	-91±22

4	-489±20	-76±12	-18±13
MDA – MDB			
	$\Delta\Sigma$	$\Delta E_{p,nb}$	ΔE_{p-m}
1	-53	7	-130
3	-24	11	-81
4	-31	-1	-18

^a The contribution associated to the interaction between the peptide and the solvent molecules (E_{p-w}), which is not explicitly listed, can be inferred from Σ and the two contributions.

Moreover, comparison between the E_{p-w} values obtained for the three peptides in MD#A (Table 3) indicates that the interaction of peptide **1** with mica is -38 kcal/mol more intense than that of peptide **4**, which in turn is significantly more favored (-73 kcal/mol) than that of peptide **3**. The affinity of peptide **1** towards the mica surface should be essentially attributed to the electrostatic interactions promoted by the guanidinium group of the arginine side group and C-terminal carboxylate group. This is clearly evidenced in Figure 7A, which depicts both a representative snapshot and the temporal evolution of the distance between the center of masses of the guanidinium group and the mica surface (d_{g-m}). In order to verify if the role-played guanidinium group is unique or other alternative peptide-surface interactions can be formed in absence of arginine, MD simulations of peptide **6** adsorbed onto mica were performed using as starting point the structure displayed in Fig. 7A. For this purpose, peptide **1** was transformed into peptide **6** by replacing arginine by alanine without changing any conformational parameter or modifying the orientation of the peptide with respect to the surface. Snapshots recorded after a few ns revealed the presence of interactions between the mica surface and both the C-terminal charged group and the glutamine polar side group (Fig. S7[†]), which is consistent with the binding observed for peptide **6**. Furthermore, the interaction involving the C-terminal charged group is fully consistent with results derived from simulations on peptide **4** adsorbed onto mica.

A completely different behavior is obtained for peptide **3**, which can be summarized as follows. First, the adsorption onto mica of the freely solvated peptide provokes an intramolecular energy penalty ($\Delta E_{p,nb}$) that is ~60% higher for peptide **3** than for peptide **1**.

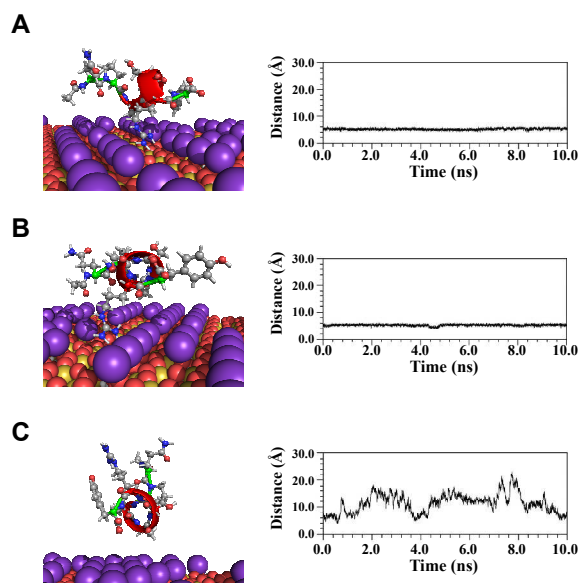


Fig. 7 Left: Snapshot of (A) **1**, (B) **3** and (C) **4** adsorbed onto mica. The displayed structures correspond to that of lowest Σ energy value (see text for the definition of Σ). Right: Temporal evolution of the distance between the center of masses of the guanidinium group and the mica substrate calculated considering the normal to the inorganic surface.

The interaction of the peptide with the inorganic substrate in MD#A simulations is $\sim 30\%$ weaker for peptide **3** than for peptide **1**. This is because in MD3A the interaction of the peptide with the substrate exclusively occurs through the arginine side group (Fig. 7). The low affinity towards mica exhibited by peptide **3** has a drastic impact on $\Delta\Sigma$, which is 29 kcal/mol (*i.e.* $\sim 65\%$) higher for peptide **3** than for peptide **1**. Indeed, the Σ values derived from MD3A are only comparable to those of MD1A when the peptide **3** adopts very stable conformations, which are infrequent presenting very short life times (*i.e.* as showed above, these conformations are entropically disfavored). Finally, the E_{p-w} term, which is very similar for MD3B and MD1B (*i.e.* -371 and -375 kcal/mol, respectively), also favors the adsorption of peptide **1** with respect to peptide **3** (*i.e.* E_{p-w} is -325 and -307 kcal/mol for MD3A and MD1A, respectively). Regarding peptide **4**, results indicate that the favorable adsorption onto mica (*i.e.* $\Delta\Sigma$ is intermediate between those calculated for peptide **1** and peptide **3**) essentially arises from the desolvation energy penalty, which is very low in relation to those obtained for the other two peptides. Thus, ΔE_{p-w} is 68, 46 and 20 kcal/mol for peptide **1**, **3** and **4**, respectively. The low ΔE_{p-w} penalty obtained for peptide **4** (*i.e.* E_{p-m} values are relatively similar for MD4A and MD4B) compensates the poor ΔE_{p-m} contribution (Table 3). Both ΔE_{p-w} and ΔE_{p-m} values are explained by the preferred binding mode found for peptide **4**. Thus, charged and polar peptide side groups are oriented towards the bulk solvent in many of the representative conformations, the main interaction with the surface involving the terminal carboxylate group only. This feature, which is clearly evidenced in the representative snapshot displayed in Fig. 7C, is also responsible of the fluctuations observed for d_{g-m} along the trajectory. Finally, in those peptide analogs in which proline is kept but the total charge of the peptide is

affected by the alanine substitution (such as peptide **6**), the capacity of such peptides to interact with the inorganic surface stems from their ability to be adsorbed without the conformational restrictions observed in peptides **1** or **3**.

Conclusions

In summary, the combined use of single molecule experiments and atomistic computer simulations allowed us to comprehend the basis of selective adsorption between a peptide selected for mica binding by phage display and mica. Using alanine scan and single molecule force spectroscopy, we noticed that the amino acid proline is highly important for the attachment of the peptide to mica. When alanine replaced proline, the adhesion of the peptide to mica reduced considerably, while replacing other amino acids in the sequence did not have any significant effect. Since proline can influence the conformation of the peptide, we assumed that this is the reason for its significant effect. FT-IR analysis supported our assumption, that the peptides has a different conformation. In addition, MD simulations on representative peptides showed that their capacity to be adsorbed on mica is closely related with their inner conformational freedom. Peptide **1**, which displays small conformational freedom, was especially influenced by the presence of a proline at its N-terminal site. Such circumstance favored its adsorption on mica, which is driven by the high affinity of peptide **1** charged groups towards mica. Specifically, both the arginine side chain and the terminal carboxylic group played a crucial role interacting with the inorganic surface. When the proline residue was replaced by alanine (peptide **3**), conformational restraints were lost affecting negatively the conformational preferences on this peptide. The adsorption, though energetically favored, became a hampered process. Upon adsorption, the internal energy of peptide **3** increased whereas the interaction with the surface was weaker than that observed for peptide **1**. This is because of the following two reasons: (1) the conformational arrangements suitable for absorption of peptide **3** only allow the side chain of arginine to actively interact with mica; and (2) the structures that facilitate the adsorption show very short life times, limiting the adsorption of peptide **3** on mica. Overall, the insights we obtained from these experimental and theoretical experiments contribute to our understanding on the interaction of peptides with inorganic surfaces. This knowledge is highly important for the development of new composite materials.

Acknowledgements

M.R acknowledges the support of Marie Curie Funds (CIG). C. A. acknowledges the financial support from the MINECO and FEDER (MAT2012-34498) and Generalitatde Catalunya (Research group 2009 SGR 925 and XRQTC). S. M acknowledges the support of the Council for Higher Education in Israel.

Notes and references

Abbreviations ND (No Detection), MD (Molecular Dynamics).

1. T. A. Horbett and J. L. Brash, *ACS Symposium Series*, Eds. 1995, **Vol. 602**, pp 1-23.
2. V. Hlady and J. Buijs, *Curr. Opin. Biotechnol* 1996, **7**, 72.

3. S. Weiner, J. Mahamid and L. Addadi, *Bone*, 2012, **50**, S19.
4. A. Miserez, J. C. Weaver, P. J. Thurner, J. Aizenberg, Y. Dauphin, P. Fratzl, D. E. Morse and F. W. Zok, *Adv. Funct. Mater.*, 2008, **18**, 1241.
5. J. Aizenberg, J. C. Weaver, M. S. Thanawala, V. C. Sundar, D. E. Morse and P. Fratzl, *Science*, 2005, **309**, 275.
6. C. A. Vilee, *N. Engl. J. Med.* 1983, **309**, 247.
7. A. Vallee, V. Humblot and C.-M. Pradier, *Acc. Chem. Res.*, 2010, **43**, 1297.
8. B. R. Peelle, E. M. Krauland, K. D. Wittrup and A. M. Belcher, *Langmuir*, 2005, **21**, 6929.
9. B. Gabryelczyk, G. R. Szilvay and M. B. Linder, *Langmuir*, 2014, **30**, 8798.
10. K. M. S. Juhl, N. Bovet, T. Hassenkam, K. Dideriksen, C. S. Pedersen, C. M. Jensen, D. V. Okhrimenko and S. L. S. Stipp, *Langmuir*, 2014, **30**, 8741.
11. J. Slocik and R. R. Naik, *Peptide-Nanoparticle Strategies, Interactions, and Challenges*, Vol. Eds.: M. R. Knecht and T. R. Walsh, Springer New York, 2014.
12. M. Sarikaya, C. Tamerler, A. K. Y. Jen, K. Schulten and F. Baneyx, *Nat. Mater.*, 2003, **2**, 577.
13. C. Tamerler and M. Sarikaya, *Acta Biomater.*, 2007, **3**, 289.
14. U. O. S. Seker and H. V. Demir, *Molecules*, 2011, **16**, 1426.
15. S. E. Feller, Y. H. Zhang, R. W. Pastor and B. R. Brooks, *J. Chem. Phys.*, 1995, **103**, 4613.
16. R. Hassert, M. Pagel, Z. Ming, T. Häupl, B. Abel, K. Braun, M. Wiessler and A. G. Beck-Sickinger, *Bioconjugate Chem.*, 2012, **23**, 2129.
17. J. B. Delehanty, K. Boeneman, C. E. Bradburne, K. Robertson, J. E. Bongard and I. L. Medintz, *Ther. Deliv.*, 2010, **1**, 411.
18. J. J. Green, E. Chiu, E. S. Leshchiner, J. Shi, R. Langer and D. G. Anderson, *Nano Lett.*, 2007, **7**, 874-879.
19. B. Grohe, J. O'Young, D. A. Ionescu, G. Lajoie, K. A. Rogers, M. Karttunen, H. A. Goldberg and G. K. Hunter, *J. Am. Chem. Soc.*, 2007, **129**, 14946.
20. K. J. L. Burg, S. Porter and J. F. Kellam, *Biomaterials*, 2000, **21**, 2347.
21. S. R. Whaley, D. S. English, E. L. Hu, P. F. Barbara and A. M. Belcher, *Nature*, 2000, **405**, 665.
22. C. Tamerler, E. E. Oren, M. Duman, E. Venkatasubramanian and M. Sarikaya, *Langmuir*, 2006, **22**, 7712.
23. O. Santos, J. Kosoric, M. P. Hector, P. Anderson and L. Lindh, *J. Colloid Interface*, 2008, **318**, 175.
24. Y. Wei and R. A. Latour, *Langmuir*, 2008, **24**, 6721-6729.
25. E. Evans and K. Ritchie, *Biophys. J.*, 1997, **72**, 1541-1555.
26. T. Micksch, N. Liebelt, D. Scharnweber and B. Schwenzer, *ACS Appl. Mater. Inter.* 2014, **6**, 7408.
27. S. V. Patwardhan, F. S. Emami, R. J. Berry, S. E. Jones, R. R. Naik, O. Deschaume, H. Heinz and C. C. Perry, *J. Am. Chem. Soc.* 2012, **134**, 6244.
28. A. A. Thyparambil, Y. Wei and R. A. Latour, *Langmuir*, 2012, **28**, 5687.
29. G. Hummer and A. Szabo, *Biophys. J.*, 2003, **85**, 5.
30. E. L. Florin, V. T. Moy and H. E. Gaub, *Science*, 1994, **264**, 415.
31. G. U. Lee, D. A. Kidwell and R. J. Colton, *Langmuir*, 1994, **10**, 354.
32. G. U. Lee, L. A. Chrisey and R. J. Colton, *Science*, 1994, **266**, 771-773.
33. P. Hinterdorfer, W. Baumgartner, H. J. Gruber, K. Schilcher and H. Schindler, *Proc. Natl. Acad. Sci. U.S.A.*, 1996, **93**, 3477.
34. A. Berquand, N. Xia, D. G. Castner, B. H. Clare, N. L. Abbott, V. Dupres, Y. Adriaensens and Y. F. Dufrêne, *Langmuir*, 2005, **21**, 5517.
35. A. Touhami, B. Hoffmann, A. Vasella, F. A. Denis and Y. F. Dufrêne, *Langmuir*, 2002, **19**, 1745.
36. V. Dupres, F. D. Menozzi, C. Locht, B. H. Clare, N. L. Abbott, S. Cuenot, C. Bompard, D. Raze and Y. F. Dufrêne, *Nat. Methods*, 2005, **2**, 631.
37. Y. Shan, J. Huang, J. Tan, G. Gao, S. Liu, H. Wang and Y. Chen, *Nanoscale*, 2012, **4**, 1283.
38. J. Landoulsi and V. Dupres, *ChemPhysChem*, 2011, **12**, 1310.
39. S. Krysiak, S. Liese, R. R. Netz and T. Hugel, *J. Am. Chem. Soc.* 2014, **136**, 688.
40. Y. Ratzvag, V. Gutkin and M. Reches, *Langmuir*, 2013, **29**, 10102.
41. S. Donatan, H. Yazici, H. Bermek, M. Sarikaya, C. Tamerler and M. Urgan, *Mat. Sci. Eng. C-Bio. S.*, 2009, **29**, 14.
42. F. A. Carvalho and N. C. Santos, *Iubmb Life*, 2012, **64**, 465.
43. A. Noy, *Curr. Opi. Chem. Biol.*, 2011, **15**, 710.
44. J. L. Hutter and J. Bechhoefer, *Rev. Sci. Instrum.*, 1993, **64**, 1868.
45. M. Jaschke and H. J. Butt, *Rev. Sci. Instrum.*, 1995, **66**, 1258.
46. E. Evans, K. Kinoshita, S. Simon and A. Leung, *Biophys. J.*, 2010, **98**, 1458.
47. Y. Duan, C. Wu, S. Chowdhury, M. C. Lee, G. M. Xiong, W. Zhang, R. Yang, P. Cieplak, R. Luo, T. Lee, J. Caldwell, J. M. Wang and P. Kollman, *J. Comput. Chem.*, 2003, **24**, 1999.
48. H. Heinz, H. Koerner, K. L. Anderson, R. A. Vaia and B. L. Farmer, *Chem. Mater.*, 2005, **17**, 5658-5669.
49. O. Bertran, D. Curco, D. Zanuy and C. Aleman, *Faraday Discuss.*, 2013, **166**, 59.
50. W. L. Jorgensen, J. Chandrasekhar, J. D. Madura, R. W. Impey and M. L. Klein, *J. Chem. Phys.*, 1983, **79**, 926.
51. J. C. Phillips, R. Braun, W. Wang, J. Gumbart, E. Tajkhorshid, E. Villa, C. Chipot, R. D. Skeel, L. Kale and K. Schulten, *J. Comput. Chem.*, 2005, **26**, 1781.
52. A. Toukmaji, C. Sagui, J. Board and T. Darden, *Journal of Chemical Physics*, 2000, **113**, 10913-10927.
53. H. C. Andersen, *J. Comput. Phys.*, 1983, **52**, 24.
54. H. J. C. Berendsen, J. P. M. Postma, W. F. Vangunsteren, A. Dinola and J. R. Haak, *J. Chem. Phys.*, 1984, **81**, 3684.
55. G. J. Martyna, D. J. Tobias and M. L. Klein, *Journal of Chemical Physics*, 1994, **101**, 4177.
56. C. Tamerler and M. Sarikaya, *Acta Biomater.*, 2007, **3**, 289.
57. H. Lee, N. F. Scherer and P. B. Messersmith, *Proc. Natl. Acad. Sci. U.S.A.*, 2006, **103**, 12999.
58. A. V. Krasnoslobodtsev, L. S. Shlyakhtenko and Y. L. Lyubchenko, *J. Mol. Biol.* 2007, **365**, 1407.
59. G. I. Bell, *Science* 1978, **200**, 618.
60. J. Kong and S. Yu, *Acta Biochim. Biophys. Sin.* 2007, **39**, 549.
61. K.A. Feeney et al. *Biopolymers*, 2003, **72**, 123.
62. M. Gupta et al. *Adv. Matter*, 2007, **19**, 858.

63. D. Zanuy, A. Flores-Ortega, J. Casanovas, D. Curco, R. Nussinov and C. Aleman, *J. Phys. Chem. B*, 2008, **112**, 8692.
64. L. Agemy, K. N. Sugahara, V. R. Kotamraju, K. Gujraty, O. M. Girard, Y. Kono, R. F. Mattrey, J.-H. Park, M. J. Sailor, A. I. Jimenez, C. Cativiela, D. Zanuy, F. J. Sayago, C. Aleman, R. Nussinov and E. Ruoslahti, *Blood*, 2010, **116**, 2847.
65. G. Revilla-Lopez, J. Torras, R. Nussinov, C. Aleman and D. Zanuy, *Phys. Chem. Chem. Phys.*, 2011, **13**, 9986.